Chinese Chemical Letters 37 (2026) 111838

Contents lists available at ScienceDirect

Chinese Chemical Letters

journal homepage: www.elsevier.com/locate/cclet

Amorphous-boron boosted Fenton-like activation of periodate for water remediation: Multiple routes for generating reactive oxygen species

Shuo Chen[a,b], Yuxuan Xiang[a,b], Qiulin Yang[c,d], Shuang Meng[a,b], Chuanshu He[a,b], Yang Liu[a,b], Jing Zhang[a,b], Zhaokun Xiong[a,b], Peng Zhou[a,b,*], Bo Lai[a,b]

[a] State Key Laboratory of Hydraulics and Mountain River Engineering, College of Architecture and Environment, Sichuan University, Chengdu 610065, China
[b] Sino-German Centre for Water and Health Research, Sichuan University, Chengdu 610065, China
[c] Sichuan Development Environmental Science and Technology Research Institute Co., Ltd., Chengdu 610095, China
[d] Sichuan Provincial Industrial Wastewater Pollution Control and Low Carbon Resource Utilization Engineering Technology Research Center, Chengdu 610095, China

ARTICLE INFO

Article history:
Received 4 June 2025
Revised 27 August 2025
Accepted 15 September 2025
Available online 16 September 2025

Keywords:
Fenton-like reaction
Boron
Fe(III)/Fe(II) circulation
Radical and nonradical pathways
Co-catalyst

ABSTRACT

Although periodate (PI) activation *via* iron-based Fenton-like reactions effectively generates reactive oxygen species (ROS) for pollutant degradation, Fe(III) accumulation poses a major challenge to sustained ROS generation. Here, amorphous-boron (AB) was employed as a co-catalyst for boosting Fenton-like activation of PI (primarily Fe(III)/PI) towards water decontamination, and the AB/Fe(III)/PI process can promptly and steadily oxidize sulfamethoxazole (SMX) during 5 cycling tests. Through integrated qualitative and semi-quantitative analyses of ROS, including EPR, quenching, and chemical probes, AB can directly activate PI to produce hydroxyl radical and indirectly accelerate Fenton-like activation of PI to produce Fe(IV) by reducing Fe(III). The synergetic routes of radical (hydroxyl radical) and non-radical (Fe(IV)) ensure the high capability of AB/Fe(III)/PI for degrading a wide variety of contaminants with diversiform molecular structures. Moreover, characterizations (XPS, EPR, HAADF-STEM, HRTEM, Raman, and XRD) reveals the stepwise boron oxidation *via* B-B bond cleavage can sustainably donate electron for direct and indirect activation of PI. The self-cleaning surface caused by the synergetic stepwise oxidation of boron and dissolution of boron oxide maintains the high stability of AB for co-catalyzing Fenton-like activation of PI during long-term operation. Therefore, this study proposes a novel Fenton-like technique for eliminating organic contaminants with low iron sludge output and long-term stability.

© 2026 Published by Elsevier B.V. on behalf of Chinese Chemical Society and Institute of Materia Medica, Chinese Academy of Medical Sciences.

The emergence of periodate (PI, IO_4^-) based advanced oxidation processes (AOPs) has become a series of new strategies for environmental remediation, owing to the exceptional stability and minimized safety concerns during storage and transportation compared with some conventional oxidants (*e.g.*, hydrogen peroxide, peracetic acid, hypochlorous acid, and persulfates) [1,2]. In general, various reactive oxygen species (ROS) generated *via* PI activation can selectively or non-selectively degrade diverse organic contaminants, including iodate radical ($^{\bullet}IO_3$), oxygen radical anion ($^{\bullet}O^-$), hydroxyl radical ($^{\bullet}OH$), singlet oxygen ($^1O_2$) [3,4]. Therefore, searching for state-of-the-art methods to activate PI for ROS generation is the core task for promoting the application of PI-based AOPs for environmental remediation.

In recent years, various strategies were thus developed to activate PI by coupling with extra energy stimulations (*e.g.*, light irradiation, ultrasound, and electricity) [5,6] and chemical activators (*e.g.*, reducing agents, carbon materials, and metal ions) [7–9]. Among these strategies, ferrous ion (Fe(II)) exhibits high capability to activate PI to generate ROS *via* Fenton-like reaction. It is different from the conventional ROS (*e.g.*, $^{\bullet}IO_3$, $^{\bullet}OH$, and $^1O_2$) derived from PI, Fe(IV) ($Fe^{IV}O^{2+}$, 2.0 V) derived from two electrons oxidation of Fe(II) species was identified as the primary ROS in Fe(II)/PI using ^{18}O isotopes labeling method and XANES analysis [10]. Fe(IV), as a high-spin state and electrophilic ROS, demonstrates strong anti-interference capabilities against common co-existing substances (*e.g.*, chloride, carbonate, and nitrate) while exhibiting remarkable selectivity for degrading electron-rich organic contaminants [11,12]. Although abundant ROS can be produced at the initial stage (Fe(II)-rich conditions) of the Fe(II)/PI

* Corresponding author.
E-mail address: zhoup1219@sina.com (P. Zhou).

https://doi.org/10.1016/j.cclet.2025.111838
1001-8417/© 2026 Published by Elsevier B.V. on behalf of Chinese Chemical Society and Institute of Materia Medica, Chinese Academy of Medical Sciences.

process, the progressive Fe(III) accumulation at the second stage caused by fast Fe(II) oxidation and unrealizable Fe(III) reduction severely restricts the sustained ROS generation for long-term degradation of organic contaminants.

To relieve Fe(III) accumulation in iron-mediated Fenton and Fenton-like systems, a wide variety of extra electron donor were used to facilitate Fe(III) reduction to Fe(II), thereby establishing sustainable Fe(III)/Fe(II) redox cycling for sustained ROS generation [13–15]. This strategy started from an accidental discovery by coupling hydroxylamine with Fenton (Fe(II)/H_2O_2) system [16], which subsequently prompted many attempts to add reducing agents into Fenton/Fenton-like systems, such as soluble organic acids (*e.g.*, L-cysteine and L-ascorbic acid) [17], sulfite [18], transition metal sulfides (*e.g.*, tungsten sulfide, molybdenum sulfide, and ferric sulfide) [19], zero valent metals (*e.g.*, zero valent tungsten) [20], and single-atom catalysts [21,22]. Although these reducing agents can rapidly reduce Fe(III) for significantly expediting Fenton/Fenton-like oxidation, their applications were also strongly limited by two factors: (i) ROS quenching effects from reducing agents and the products resulting from their decomposition (*e.g.*, hydroxylamine, L-cysteine, and L-ascorbic acid); (ii) decomposition of reducing agents caused metal leaching or organic pollution [23]. Seeking for a suited electron donor is thus an exigent task for achieving long-term and green Fenton-like activation of PI.

Boron powder may be an ideal electron donor to facilitate direct Fe(III) reduction for long-lasting and green future of Fenton-like activation of PI [24,25]. Positioned between beryllium and carbon in the periodic table, boron displays semi-metallic characteristics due to its intermediate electronegativity and specific electronic configuration ($1s^2 2s^2 2p^1$) [26,27]. This specific property makes boron easily donate electron to induce reduction reactions, meanwhile, the oxidative corrosion of boron with stepwise oxidation from B^0 to B^{3+} can sustainably provide electron. For instance, previous reports unveiled that both amorphous- and crystal-boron can effectively activate peroxymonosulfate (PMS) through direct electron donation, cleaving the asymmetric O-O bond to generate ROS for degrading refractory organic pollutants (*e.g.*, phthalates) [28,29]. Therefore, due to the high-efficiency of boron for donating electron, boron as a green electron- sacrificial agent shows high potential for directly reducing Fe(III) and accelerating Fenton-like activation of PI without secondary organic/metal pollution.

This study is aimed to develop a sustainable strategy for boosting Fenton-like activation of PI, while amorphous-boron (AB) was applied as the co-catalyst and sulfamethoxazole (SMX) was employed as the primary target pollutant. Both amorphous- and crystal-boron exhibit high-performance to boost Fe(III)/PI to degrade SMX. The performance and mechanism of the AB/Fe(III)/PI system were deeply investigated *via* ROS analysis (quenching tests, chemical probe tests, electron paramagnetic resonance (EPR) analysis, and broad-spectrum tests), iron species transformation, and characterizations (X-ray photoelectron spectroscopy (XPS), EPR, high-angle annular dark-field scanning transmission electron microscopy (HAADF-STEM), high-resolution transmission electron microscopy (HRTEM), Raman spectroscopy, and X-ray diffraction (XRD)). Moreover, the long-term stability of AB for co-catalyzed Fenton-like PI activation was explored by 5 consecutive cycling tests.

The details of all chemicals, analysis and characterization methods were provided in Texts S1-S6 (Supporting information).

Fig. 1 depicts the co-catalytic reactivity of amorphous-boron (AB) for boosting iron species mediation Fenton-like activation of PI for SMX degradation. As shown in Fig. 1a, SMX cannot be directly oxidized by PI alone, and meanwhile, the reactivity of Fe(III) for activating PI can also be ignored due to the low removal ratio of SMX (<10%) at 30 min in Fe(III)/PI. Although Fe(II) can effectively activate PI to degrade SMX, only 14.4% was removed in

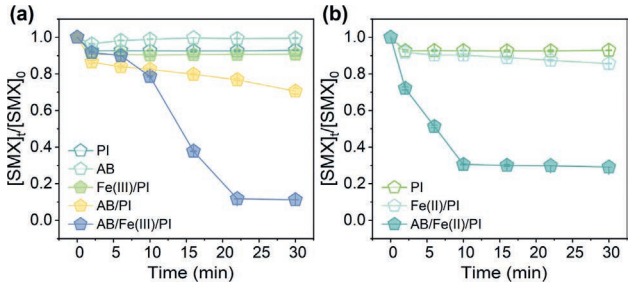


Fig. 1. SMX degradation in AB assisted Fenton-like systems: (a) Fe(III)/PI and (b) Fe(II)/PI.

Fe(II)/PI with low dosage of Fe(II) (25 μmol/L) (Fig. 1b). Moreover, AB exhibits the effective reactivity to directly activate PI, resulting from that almost 30% SMX was degraded at 30 min in AB/PI. To our delight, nearly 90% SMX was removed by coupling AB and Fenton-like activation of PI (both Fe(III)/PI and Fe(II)/PI). Notably, the overall degradation efficiency of SMX in the AB/Fe(II)/PI system was lower than in AB/Fe(III)/PI, attributed to rapid oxidant consumption causing inefficient radical utilization (Fig. S1 in Supporting information). The AB dosage was optimized at 100 mg/L (Fig. S2 in Supporting information), where SMX degradation efficiency plateaued with complete periodate decomposition (Fig. S1). However, the performance of crystal-boron (CB) for co-catalyzing Fe(III)/PI is significantly lower than that of AB (Fig. S3 in Supporting information). Therefore, AB shows its activity to boost Fe/PI *via* the synergetic direct activation and indirect Fenton-like activation of PI.

Previous literatures reported the generation of multiple ROS during Fenton-like activation of PI [10,30], various analytical approach were employed to identify and quantify the generation of ROS in AB/Fe(III)/PI, including EPR using 5,5-dimethyl-1-pyrroline *N*-oxide (DMPO) for radical trapping and 4-amino-2,2,6,6-tetramethylpiperidine (TEMP) for singlet oxygen detection, chemical probe tests (coumarin (COU) for $^{\bullet}OH$ and methyl phenyl sulfoxide (PMSO) for Fe(IV)) as well as quenching tests (methyl alcohol (MeOH) for reactive radicals). Above all, the generation of reactive radicals was qualitatively detected by EPR under the capturing of DMPO. Fig. 2a depicts that the characteristic EPR spectrum of DMPO-OH adducts was clearly detected in the EPR spectrum obtained from AB/PI, indicating the reactivity of AB for directly activating PI and generating hydroxyl radicals (Eq. 1) [31]. It further confirms with the effective oxidation of SMX in AB/PI (Fig. 1a). Moreover, the EPR spectrum of AB/Fe(III)/PI showed a higher DMPO-OH adduct intensity compared to AB/PI, indicating the generation of hydroxyl radicals and that Fe(III) significantly accelerates this process. Although previous studies proposed that singlet oxygen can also be generated *via* PI induced chain reactions (Eqs. 2–4) [32,33], the absence of characteristic TEMP-$^1O_2$ adduct signals in the EPR spectra of both AB/PI and AB/Fe(III)/PI systems conclusively excludes singlet oxygen as the predominant reactive oxygen species in AB/Fe(III)/PI (Fig. S4 in Supporting information).

For further investigating the generation of hydroxyl radicals in AB/Fe(III)/PI, chemical probe test using COU as the trapping agent was performed by quantitatively detecting the specific product (7-hydroxycoumarin (7-HC)) of hydroxyl radical induced oxidation of COU [34,35]. As shown in Fig. 2b, the concentration of 7-HC increased with the reaction progress and 0.7 μmol/L 7-HC was measured at 30 min in AB/Fe(III)/PI, further confirming the generation of hydroxyl radicals in AB/Fe(III)/PI. Moreover, to analyze the contribution of hydroxyl radicals for SMX degradation, the quenching tests with MeOH ($k(MeOH, {}^{\bullet}OH) = 9.7 \times 10^8\ mol\ L^{-1}\ s^{-1}$) as the quenching agent were carried out in both AB/PI and AB/Fe(III)/PI

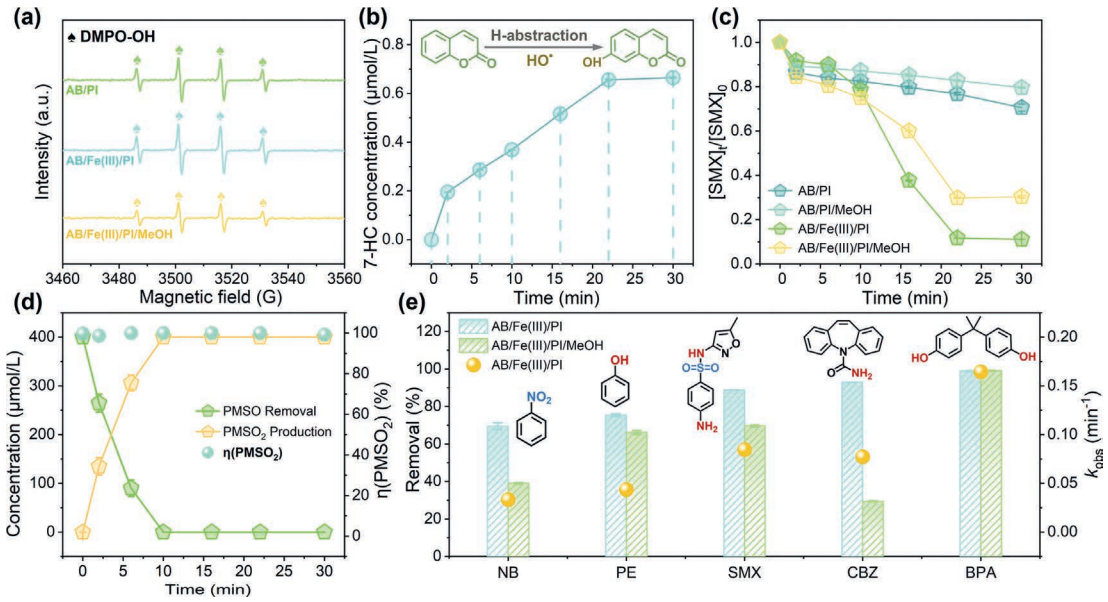


Fig. 2. (a) EPR analysis of different systems, (b) ·OH analysis using COU as chemical probe, (c) MeOH quenching effects on SMX degradation, (d) Fe(IV) detection *via* PMSO as chemical probe, (e) degradation kinetics of contaminants in AB/Fe(III)/PI.

[36]. Fig. 2c depicts that SMX removal ratio decreased from 29.4% to 20.4% in AB/PI when treated with high concentration of MeOH (10 mmol/L), and meanwhile, it decreased from 88.9% to 70.0% in AB/Fe(III)/PI by adding MeOH. Combined with the results of EPR tests and chemical probe test, the effective inhibition effect of MeOH proves the contribution of hydroxyl radicals for SMX degradation in both AB/PI and AB/Fe(III)/PI. However, it was detected nearly 90% SMX was degraded in AB/Fe(III)/PI (Fig. 1a), which is not matched well with the low output of 7-HC and the faint inhibition effect of MeOH. These results explain the potential that another ROS may be produced for oxidizing organic contaminants in AB/Fe(III)/PI.

Recent studies have identified Fe(IV) as the main ROS in Fe(II)-activated PI systems, a semi-quantitative analysis using PMSO as chemical probe was also carried out [10,25]. Due to the distinctive oxygen transfer mechanism from Fe(IV) to PMSO to form methyl phenyl sulfone ($PMSO_2$) [12,37], the quantitative measurement of $PMSO_2$ in AB/Fe(III)/PI can identify the formation of Fe(IV) and its contribution for eliminating organic contaminants. As can be seen in Fig. 2d, PMSO was gradually degraded with the generation of $PMSO_2$ during reaction progress, indicating the generation of Fe(IV) *via* Eq. 5 in AB/Fe(III)/PI. It should be noted that PMSO was almost completely degraded within 10 min, which reveals the high output of Fe(IV) for water decontamination. Moreover, the conversion ratio from PMSO to $PMSO_2$ ($\eta(PMSO_2) = \Delta[PMSO_2]/\Delta[PMSO]$) maintained at almost 100% during whole reaction progress. Due to the high reactivity between Fe(IV) and PMSO ($k = 1.23 \times 10^5$ mol L^{-1} s^{-1}) [38], these phenomena indicate synergistical effect of high proportion of Fe(IV) output and substrate specific reactivity of AB/Fe(III)/PI. The results of the qualitative and semi-quantitative analysis indicate that hydroxyl radicals and Fe(IV) were synergistically generated for degrading contaminants in AB/Fe(III)/PI.

$$IO_4^- + B^0 + H^+ \rightarrow IO_3^- + {}^{\bullet}OH \quad (1)$$

$$3IO_4^- + OH^- \rightarrow 3IO_3^- + 2{}^{\bullet}O_2^- + H_2O \quad (2)$$

$$IO_4^- + 2{}^{\bullet}O_2^- + H_2O \rightarrow IO_3^- + 2OH^- + 2{}^1O_2 \quad (3)$$

$$2{}^{\bullet}O_2^- + H_2O \rightarrow {}^1O_2 + H_2O_2 + 2OH^- \quad (4)$$

$$Fe(II) + IO_4^- \rightarrow Fe^{IV}O^{2+} + IO_3^- \quad (5)$$

$$2B^0 + 6Fe^{III} + 3H_2O \rightarrow B_2O_3 + 6Fe^{II} + 6H^+ \quad (6)$$

$$B_2O_3 + 6H_2O \rightarrow 2H_3BO_3 + 6H^+ \quad (7)$$

The synergistic generation of hydroxyl radicals and Fe(IV) in AB/Fe(III)/PI leads to substrate specific degradation kinetics, resulting from the diversity of second-order rate constants of hydroxyl radical and Fe(IV) for the oxidization of organic contaminants (Table S2 in Supporting information) [23,39–42]. While hydroxyl radicals exhibit rapid, non-selective oxidation of organic contaminants with high rate constants ($>10^9$ mol L^{-1} s^{-1}), the quenching effects of co-existing substrates (*e.g.*, halide ions, metal ions, and organic matter) strongly decrease the utilization efficiency of hydroxyl radicals and their precursors [11,12]. In contrast to hydroxyl radical, Fe(IV) can immune largely from these co-existing substrates to degrade some electron rich contaminants with moderate reaction rate constants (10^3–10^5 mol L^{-1} s^{-1}), however, it cannot effectively degrade some refractory organic contaminants (*e.g.*, nitrobenzene (NB) and benzoic acid (BA)) [12]. As depicted in Fig. 2e and Fig. S5 (Supporting information), although the contribution percentages of hydroxyl radical and Fe(IV) for degrading contaminant were significantly different (identified by adding 10 mmol/L MeOH to quenching hydroxyl radical), the AB/Fe(III)/PI process can effectively and rapidly degrade various contaminants with absolutely different molecular structures (NB (0.033 min^{-1}), phenol (PE, 0.044 min^{-1}), SMX (0.085 min^{-1}), carbamazepine (CBZ, 0.077 min^{-1}), and bisphenol A (BPA, 0.164 min^{-1}). Using the frontier orbital energies (E_{HOMO}, reflecting the electron-donating capacity of the molecule) and vertical ionization potential (VIP, correlating with compound reactivity) as molecular descriptors (Table S3 in Supporting information) [43], contaminants with higher E_{HOMO} values and lower VIP values undergo accelerated degradation rates (Fig. S6 in Supporting information). This trend is consistent with the selectivity of Fe(IV)-mediated oxidation toward

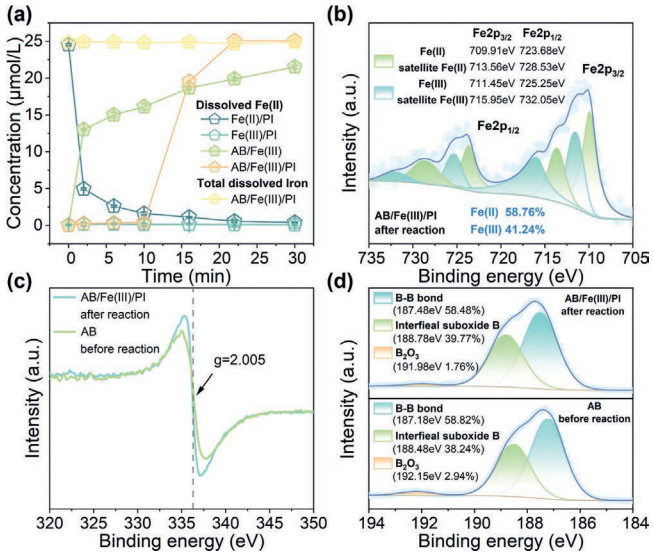


Fig. 3. (a) Fe species transformation in AB mediated systems, (b) high-resolution Fe 2p spectrum of reacted AB, (c) EPR spectra and (d) high-resolution B 1s spectrum of original and reacted AB in AB/Fe(III)/PI.

electron-rich moieties. However, the inferior linear relationship between k_{obs} and E_{HOMO}/VIP may be ascribed to the non-selective degradation pathway involving hydroxyl radicals [44]. For this reason, the AB/Fe(III)/PI process can synergistically degrade organic contaminant *via* both radical (hydroxyl radical) and non-radical (Fe(IV)) approaches, overcoming the drawbacks of single ROS dominated oxidation process. Therefore, the AB/Fe(III)/PMS system demonstrates significant potential for practical application, effectively degrading SMX in real water matrixes of tap water, river water (Jiang'an River, Chengdu), and lake water (Mingyuan Lake, Sichuan University), as shown in Fig. S7 (Supporting information).

Generally, the iron mediated Fenton-like chain reaction is fundamentally governed by the cyclic conversion between Fe(III) and Fe(II), where ROS generation is rate-limited by the Fe(III) reduction step [23]. As shown in Fig. 3a, Fe(II) was converted to Fe(III) in Fe(II)/PI within 15 min due to the rapid oxidation of Fe(II) by PI to produce Fe(IV) *via* Eq. 5, while the Fe(III)/PI system showed negligible Fe(II) production during whole reaction indicating the low activity of PI to reduce Fe(III). Notably, AB exhibits exceptional Fe(III) reduction capability, while >20 μmol/L Fe(II) was detected after 30 min reaction in the AB/Fe(III). Nearly all iron species stayed dissolved state in AB/Fe(III)/PI, indicating low adsorption capability of AB towards iron species. Although rapid oxidation of Fe(II) by sufficient PI in AB/Fe(III)/PI prevented detection of Fe(II) within the first 10 min, Fe(II) concentration promptly increase to 25 μmol/L in the following 10 min due to PI consumption. XPS spectra (Fig. S8 in Supporting information) reveal that elements of boron and oxygen were detected on the surface or pristine AB powder, while a small amount of residual iron was detected on the surface of reacted AB powder in AB/Fe(III)/PI. The high-resolution Fe 2p spectrum of reacted AB powder (Fig. 3b) confirms Fe(III) reduction (Eq. 6) on its surface due to the synchronous appearance of Fe(II) (58.76 %, 709.91 eV and 723.68 eV) and Fe(III) (41.24 %, 711.45 eV and 725.25 eV) [24,44]. The simultaneous Fe(III) reduction and Fe(II) oxidation occurring on the AB surface guarantee the Fe(III)/Fe(II) circularly catalyzed Fenton-like activation of PI to produce ROS.

Above results indicate that AB induced Fe(III) reduction is critical for ROS formation in Fenton-like activation of PI, the electron-donation mechanism of AB was thus investigated by EPR, B 1s XPS spectra, and HAADF-STEM images of pristine AB and reacted AB. As shown in Fig. 3c, the high intensity of unpaired electron ($g = 2.005$) exhibits the high-performance for AB to reduce Fe(III) [44], and meanwhile, almost no attenuation of the high intensity of unpaired electron was detected resulting in the long-term stability of AB for co-catalyzing Fenton-like activation of PI. The high-resolution B 1s spectrum (Fig. 3d) of pristine AB demonstrates three types of boron species on the AB surface, including unoxidized boron in the form of B-B bonds (B^0 at 187.18 eV, 58.82 %), interfacial suboxide boron (B^+ and B^{2+} at 188.48 eV, 38.24 %) as well as boron oxide (B^{3+} at 192.15 eV, 2.94 %) [24,45]. Among these boron species, low valent boron species (B^0, B^+, and B^{2+}) generally exhibit electron-donation ability for Fe(III) reduction, while boron oxide cannot effectively reduce Fe(III) [24,46]. It should be noted that the proportions of boron specie (unoxidized boron (58.48 %), interfacial suboxide boron (39.77 %), and boron oxide (1.76 %)) on the surface of reacted AB did not significantly change, resulting from the stepwise oxidation of boron species to form boron oxide, which is readily soluble in water solution.

HRTEM images (Figs. 4a and b) of pristine AB clearly illustrate the simultaneous appearance of crystal regions and amorphous regions on the surface of AB, indicating that AB is ordered within short-range (constituted by well-ordered B_{12} icosahedra) and disordered in long-range [26,29]. The lattice spacings of some crystal regions on AB surface are 0.236 nm and 0.262 nm. The amorphous regions constituted by interfacial suboxide boron and boron oxide appear at the edge of pristine AB. The short-range-ordered and long-range-disordered property of reacted AB was also measured with the lattice spacings of 0.235 nm and 0.254 nm (Figs. 4c and d). Moreover, high-definition HAADF-STEM image of pristine AB (Fig. 4e) shows clear surface outline. However, Fig. 4f depicts that the amorphous regions on the surface of reacted AB obviously increased after reaction in AB/Fe(III)/PI, resulting from the cleavage of B-B bonds to form interfacial suboxide boron and boron oxide [46]. It should be particularly noted that the distribution of iron on the surface of reacted AB matches well with the emerging disordered regions based on HAADF-STEM image (Fig. 4g) and energy-dispersive X-ray (EDX) mapping (Fig. 4h). This phenomenon further reveals that the low-valent boron sites significantly contribute to Fe(III) reduction by cleaving B-B bonds to donate electrons, with concomitant destruction of the surface structure of AB and generation of interfacial suboxide boron and boron oxide. Therefore, stepwise corrosion of AB ensures a continuous electron source for Fe(III) reduction, leading to a long-lasting generation of hydroxyl radicals and Fe(IV) for water decontamination in AB/Fe(III)/PI.

The effectiveness of iron-mediated Fenton-like oxidation processes in degrading organic contaminants is generally pH-dependent, primarily because the hydrolysis of Fe(II) and Fe(III) species alters the reaction kinetics [47]. Fig. 5a shows the pH-dependence of SMX degradation by AB/Fe(III)/PI. The AB/Fe(III)/PI process can nearly absolutely degrade SMX in 20 min at pH ranging from 2.0 to 2.8. The SMX removal ratio gradually decreased with the increasing initial pH from 3.0 to 5.0 and became negligible at pH ≥ 4.2 in AB/Fe(III)/PI. To further analyze the mechanism of iron species mediated pH-dependent performance of AB/Fe(III)/PI, the distribution fractions of various Fe(II) species (derived from the hydrolysis of Fe(II)) (Fig. S9 in Supporting information) and various Fe(III) species (derived from the hydrolysis of Fe(III)) (Fig. 5b) were calculated at pH ranging from 1.0 to 6.0, which were then matched with k_{obs} of SMX removal in AB/Fe(III)/PI.

At the pH range of 1.0–6.0, the dominant form of Fe(II) is Fe^{2+} (distribution fraction > 99.99 %),which shows no correlation with k_{obs} of SMX removal, indicating that the form of Fe(II) species is not the origin of pH-dependent performance of AB/Fe(III)/PI. However, at pH 1.0~6.0, the main Fe(III) species include Fe^{3+}, $FeOH^{2+}$, and $Fe(OH)_2^+$ [48], more importantly, the sum value of

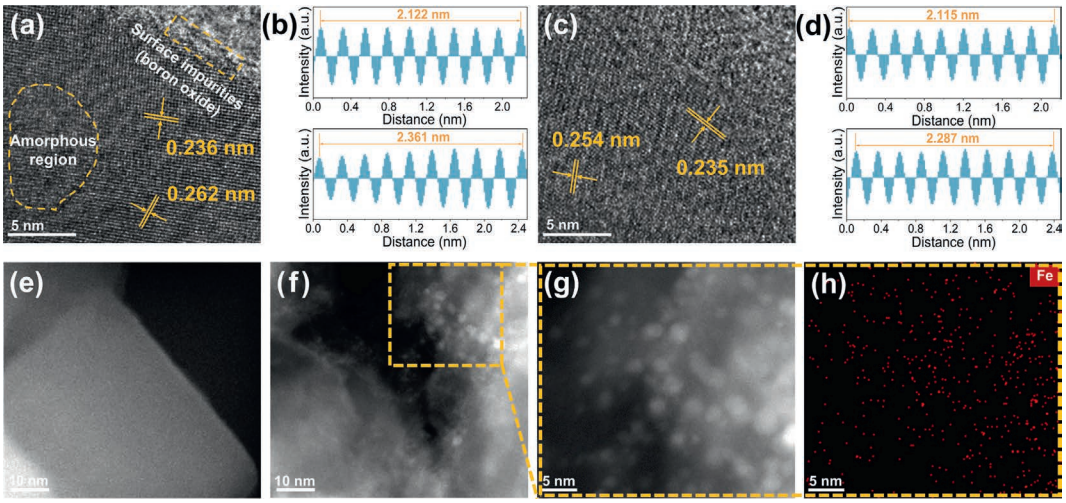


Fig. 4. HRTEM images and the corresponding extracted line profiles of (a, b) original AB and (c, d) reacted AB (5 cycles), (e) HAADF-STEM images of original AB, (f, g) HAADF-STEM images and (h) EDX elemental mapping of reacted AB (5 cycles).

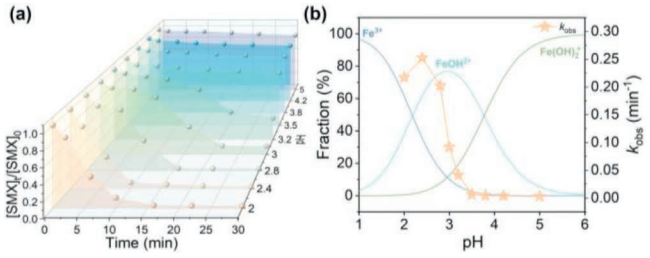


Fig. 5. (a) Temporal profiles of SMX removal under various initial pH in AB/Fe(III)/PI, (b) contrast between k_{obs} of SMX removal and Fe(III) morphology distribution (quantified by Visual MINTEQ modeling) at pH ranging from 1.0 to 6.0.

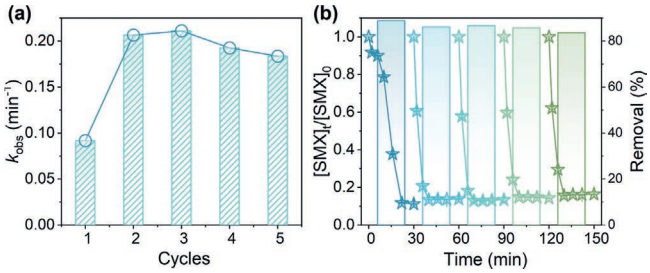


Fig. 6. (a) k_{obs} (initial 15 min) and (b) ratios of degradation of SMX in the Cycling tests of AB powder.

Fe^{3+} and $FeOH^{2+}$ is highly correlated to the k_{obs} of SMX removal in AB/Fe(III)/PI. Therefore, the rate-limiting step of AB-mediated reduction of Fe(III) species (primarily in the form of Fe^{3+} and $FeOH^{2+}$) causes the pH-dependent performance of AB/Fe(III)/PI for degrading organic contaminants.

The stability of co-catalyst for long-term operation serves as a key factor in advancing its progression from scientific research to practical application. Thus, the long-term stability of AB concerning its co-catalytic performance for Fe(III)/PI was assessed using cycling tests. As depicted in Fig. 6, the overall removal efficiencies of SMX in AB/Fe(III)/PI during 5 cycling tests keep almost unchanged (>85 %), indicating the high stability of AB for long-term operation. The Raman spectra of pristine AB and reacted AB demonstrate that the surface bonds of AB maintain similar compositions before and after reaction in AB/Fe(III)/PI (Fig. S10 in Supporting information), which ensures the high reactivity of AB during cycling tests. Moreover, it should be noted that the k_{obs} of SMX removal at initial 15 min in cycling test 1 (0.092 min^{-1}) is significantly lower than those obtained from cycling test 2 to 5 (0.207, 0.211, 0.193, 0.184 min^{-1}). Although the surface boron oxide (B_2O_3) can be hydrolyzed into water (H_2BO_3) for exposing highly reactive low-valent boron species for Fe(III) reduction (Eq. 7) [46], the boron oxide partially covered on the surface of AB also delays Fe(III) reduction to cause the tardive SMX degradation at initial 10 min in cycling test 1. It is confirmed with the relatively higher content of boron oxide in B 1s XPS spectrum of pristine AB (Fig. 3d) and lower XRD intensity of crystal boron regions of pristine AB (Fig. S11 in Supporting information). Based on above results, the self-cleaning effect caused by the synergetic stepwise oxidation of boron and dissolution of boron oxide maintains the high stability of AB for co-catalyzing Fenton-like activation of PI during long-term operation.

Fe(II) as an environmentally friendly catalyst can effectively activate PI to generate ROS for the elimination of organic contaminants, however, the fast accumulation of Fe(III) critically hinders the long-lasting generation of ROS in the Fe(II)/PI reaction. In this work, AB was applied as co-catalyst to enhance the Fe(III)/PI reaction with SMX as the primary contaminant. The AB/Fe(III)/PI process displays high performance to degrade SMX with high stability during cycling tests. Mechanism investigations (ROS analysis and characterization) reveal that AB serves dual functions as an activator and a co-catalyst to boosting Fe(III)/PI *via* two routes: (i) Directly activating PI to produce hydroxyl radicals; (ii) indirectly promoting Fenton-like activation of PI to produce Fe(IV) by accelerating Fe(III) reduction. The simultaneous generation of hydroxyl radicals and Fe(IV) in AB/Fe(III)/PI enables synergistic degradation *via* both radical and non-radical pathways, overcoming the limitations of single ROS dominated oxidation processes. Moreover, compared to other electron-sacrificial agent (*e.g.*, L-cysteine, ascorbic acid, metal sulfides, and zero-valent metals), AB as an inorganic non-metallic material, essentially avoids environmental risks caused by secondary organic pollution/transition metal leaching. Its self-cleaning surface maintains the continuously refresh of active boron sites for long-term stability during cyclic tests. Therefore, the enhanced Fenton-like system coupling AB with Fe(III)/PI exhibits significant potential for sustainable water decontamination through persistent ROS generation with minimal iron sludge production. For extended water treatment applications, periodic AB supplementation could be considered to compensate for its gradual sacrificial consumption, thereby ensuring long-term system efficacy.

Declaration of competing interest

The authors declare that they have no known competing financial interests or personal relationships that could have appeared to influence the work reported in this paper.

CRediT authorship contribution statement

Shuo Chen: Writing – review & editing, Writing – original draft, Software, Methodology, Investigation, Formal analysis, Data curation. **Yuxuan Xiang:** Writing – original draft, Methodology, Investigation, Formal analysis, Data curation. **Qiulin Yang:** Resources, Formal analysis. **Shuang Meng:** Investigation, Formal analysis. **Chuanshu He:** Supervision, Formal analysis. **Yang Liu:** Supervision, Formal analysis. **Jing Zhang:** Investigation, Formal analysis. **Zhaokun Xiong:** Supervision, Project administration. **Peng Zhou:** Writing – review & editing, Writing – original draft, Supervision, Project administration, Investigation, Data curation. **Bo Lai:** Writing – review & editing, Project administration, Funding acquisition.

Acknowledgments

This research was supported financially by National Natural Science Foundation of China (No. U24A20561) and Sichuan Science and Technology Program (No. 2024NSFTD0014).

Supplementary materials

Supplementary material associated with this article can be found, in the online version, at doi:10.1016/j.cclet.2025.111838.

References

[1] Q. Tang, B. Wu, X. Huang, et al., Nat. Commun. 15 (2024) 9549.
[2] L. Chen, J. Hu, A.G.L. Borthwick, et al., Nat. Water 2 (2024) 453–463.
[3] Y. Sun, Z. Fang, X. Huang, et al., Appl. Catal. B: Environ. 337 (2023) 122994.
[4] J. Du, S. Tang, Faheem, et al., Chem. Eng. J. 369 (2019) 1034–1039.
[5] F. Liu, Z. Li, Q. Dong, et al., Environ. Sci. Technol. 56 (2022) 4413–4424.
[6] M. Luo, H. Zhang, Y. Shi, et al., Water Res. 240 (2023) 120128.
[7] L. Niu, J. Lin, W. Chen, et al., Environ. Sci. Technol. 57 (2023) 7051–7062.
[8] J. Peng, P. Zhou, H. Zhou, et al., Environ. Sci. Technol. 57 (2023) 10804–10815.
[9] H. Sun, F. He, W. Choi, Environ. Sci. Technol. 54 (2020) 6427–6437.
[10] Y. Zong, Y. Shao, Y. Zeng, et al., Environ. Sci. Technol. 55 (2021) 7634–7642.
[11] S. Liang, L. Zhu, J. Hua, et al., Environ. Sci. Technol. 54 (2020) 6406–6414.
[12] Z. Wang, W. Qiu, S.-y. Pang, et al., Environ. Sci. Technol. 56 (2022) 1492–1509.
[13] S. Meng, P. Zhou, Y. Sun, et al., Water Res. 218 (2022) 118412.
[14] Z. Wang, Y. Du, P. Zhou, et al., Chem. Eng. J. 454 (2023) 140096.
[15] L. Lai, H. Zhou, Y. Hong, et al., Chin. Chem. Lett. 35 (2024) 108580.
[16] L. Chen, J. Ma, X. Li, et al., Environ. Sci. Technol. 45 (2011) 3925–3930.
[17] X. Huang, X. Hou, F. Jia, et al., ACS Appl. Mater. Interfaces 9 (2017) 8751–8758.
[18] D. Li, D. Chen, Y. Yao, et al., Chem. Eng. J. 288 (2016) 806–812.
[19] M. Xing, W. Xu, C. Dong, et al., Chem 4 (2018) 1359–1372.
[20] L. Yang, C. Hai, X. Hao, et al., Sep. Purif. Technol. 316 (2023) 123780.
[21] K. Zhu, W. Qin, Y. Chen, et al., Nano Today 58 (2024) 102462.
[22] K. Zhu, X. Liang, Y. Chen, et al., Coord. Chem. Rev. 519 (2024) 216110.
[23] H. Zhou, H. Zhang, Y. He, et al., Appl. Catal. B: Environ. 286 (2021) 119900.
[24] P. Zhou, W. Ren, G. Nie, et al., Angew. Chem. Int. Ed. 59 (2020) 16517–16526.
[25] W. Li, D. Zhou, H. Jiang, et al., Sep. Purif. Technol. 346 (2024) 127509.
[26] B. Albert, H. Hillebrecht, Angew. Chem. Int. Ed. 48 (2009) 8640–8668.
[27] T. Ogitsu, E. Schwegler, G. Galli, Chem. Rev. 113 (2013) 3425–3449.
[28] W. Ren, P. Zhou, G. Nie, et al., Water Res. 186 (2020) 116361.
[29] X. Duan, W. Li, Z. Ao, et al., J. Mater. Chem. A 7 (2019) 23904–23913.
[30] Y. Zong, H. Zhang, Y. Shao, et al., J. Hazard. Mater. 423 (2022) 126991.
[31] L. Wang, X. Lan, W. Peng, Z. Wang, J. Hazard. Mater. 408 (2021) 124436.
[32] Z. Dong, H. Guo, Y. Yang, et al., Chem. Eng. J. 502 (2024) 157977.
[33] Y. Chen, Y. Qiu, T. Chen, H. Wang, ACS Nano 19 (2025) 6588–6600.
[34] P. Zhou, J. Zhang, Z. Xiong, et al., Appl. Catal. B: Environ. 265 (2020) 118264.
[35] X. Li, Y. Liu, J. Wei, et al., Chin. Chem. Lett. 36 (2025) 110811.
[36] G.V. Buxton, C.L. Greenstock, W.P. Helman, A.B. Ross, J. Phys. Chem. Ref. Data 17 (1988) 513–886.
[37] Z. Wang, W. Qiu, S.-y. Pang, et al., Chem. Eng. J. 371 (2019) 842–847.
[38] Z. Wang, J. Jiang, S. Pang, et al., Environ. Sci. Technol. 52 (2018) 11276–11284.
[39] S.P. Mezyk, W.J. Cooper, K.P. Madden, D.M. Bartels, Environ. Sci. Technol. 38 (2004) 3161–3167.
[40] C. Luo, M. Feng, T. Zhang, V.K. Sharma, C. Huang, ACS ES&T Water 1 (2021) 969–979.
[41] S. Mandal, J. Adv. Oxid. Technol. 21 (2018) 178–195.
[42] H. Dong, Y. Li, S. Wang, et al., Environ. Sci. Technol. Lett. 7 (2020) 219–224.
[43] W. Shi, C. Zhang, H. Zhao, et al., Water Res. 266 (2024) 122428.
[44] P. Zhou, S. Meng, M. Sun, et al., Sep. Purif. Technol. 317 (2023) 123860.
[45] B. Feng, J. Zhang, Q. Zhong, et al., Nat. Chem. 8 (2016) 564–569.
[46] P. Zhou, Y. Yang, W. Ren, et al., Appl. Catal. B: Environ. 319 (2022) 121916.
[47] Y. Zhang, M. Zhou, J. Hazard. Mater. 362 (2019) 436–450.
[48] A. Stefansson, Environ. Sci. Technol. 41 (2007) 6117–6123.